BSGLg, 61, 2013, 5-14

RAINFALL RETRIEVAL USING SPINNING ENHANCED VISIBLE AND INFRARED IMAGER (SEVIRI-MSG) AND CLOUD PHYSICAL PROPERTIES (CPP) ALGORITHM: VALIDATION OVER BELGIUM AND APPLICATIONS

Julien BEAUMET, Nicolas CLERBAUX, Xavier FETTWEIS & Michel ERPICUM

Abstract
Precipitation is the main variable of the water cycle and a driving factor of the water resources availability. However, direct precipitation measurements are still too scarce to quantify the ongoing changes and to provide data for numerical models validation. Recently, Roebeling & Holleman (2009) have presented the Cloud Physical Properties (CPP) algorithm which is based on the solar channel from the SEVIRI instrument on board of the Meteosat Second Generation satellite. In this work, the authors have validated the algorithm over the Netherlands thanks to a 2-month comparison with weather radar data in summertime. The goal of the present study is to extend previous validations of the CPP and verify the algorithm performances throughout yearly and daily cycles over Belgium with the aim of identifying possible uses and applications as model validation. To do so, a seven-years data set of clouds and precipitation data over Western Europe has been generated using the CPP algorithm and analyzed. A comparison with weather radar data from the Belgian network has been performed. Results are encouraging for both precipitation areas delimitation and rain rates assessment. However, the rain rate estimation appears to be affected by the sun zenith angle with significant overestimation when this angle exceeds 60°. Systematic errors also affect the retrieval of cloud properties for thick clouds which leads to an overestimation of extreme precipitation events.

Keywords
Precipitation measurement, CPP algorithm, Meteosat Second Generation, clouds microphysics, sun zenith angle, parallax-shift correction, validation

Résumé
Les précipitations jouent un rôle déterminant dans le cycle de l'eau et pour la disponibilité de cette ressource. Malgré différentes méthodes développées, les mesures restent insuffisantes pour quantifier les changements en cours ainsi que pour la validation des modèles numériques. Récemment, Roebeling & Holleman (2009) ont présenté l'algorithme Cloud Physical Properties (CPP) qui utilise les données de l'instrument SEVIRI à bord de Météosat Seconde Génération pour l'estimation des précipitations. Dans cet article, les auteurs ont validés l'algorithme grâce à une comparaison de données acquises durant deux mois en période estivale avec les données du réseau de radars météorologiques des Pays-Bas. L'étude présentée ici étend les validations précédentes afin de vérifier les performances de l'algorithme au cours des cycles journaliers et saisonniers et permet d'identifier les limitations et applications possibles de la méthode. Un set de sept ans de données sur les nuages et les précipitations a donc ainsi été créé pour l'Europe de l'Ouest. Une comparaison avec les données du réseau belge de radars météorologiques a ensuite été effectuée. Les résultats sont encourageants à la fois pour la délimitation des zones de pluie ainsi que pour l'estimation des taux de précipitations. Cependant, ces derniers sont largement affectés par la valeur de l'angle solaire zénithal. Une surestimation significative apparaît dès que celui-ci devient supérieur à 60°. Par ailleurs, des erreurs systématiques apparaissent également pour les nuages très épais entrainant une surestimation des évènements extrêmes de précipitation.

Mots-clés
Mesure des précipitations, algorithme CPP, Météosat Seconde Génération, microphysique des nuages, angle solaire zénithal, correction de la parallaxe, validation

I. INTRODUCTION

A. Context

Fallen quantities of precipitation are a driving variable for the water cycle and the amount of water available. Moreover, highlighted within the context of global changes and growing populations, water resources availability is likely to become an important challenge for most societies over the XXIst century. Indeed, even thought there are some uncertainties concerning the pattern of precipitation changes at regional scale, it is admitted that an intensification of the water cycle is projected at middle and high latitudes with more frequent severe droughts and violent floods (Lehner *et al.,* 2006; Alexander *et al.,* 2006). Nevertheless, the lack of reliable and frequent precipitation measurements remains an obstacle for the assessment and quantification of such phenomenons (Trenberth *et al.,* 2007).

These uncertainties concerning precipitation changes are also partly explained by the difficulties for the models to simulate the precipitation formation processes. These difficulties are present for both the modelling of trends at the climate scale as well as for short range forecasting. Moreover, cloud and precipitation properties have also influences on the Earth radiation budget by modifying the amount of solar visible radiation received at the surface as well as the downward infrared radiation (Twomey, 1991). The effects of clouds on radiation are dependent of the height, optical thickness, droplet size distribution... Therefore, a better understanding of precipitation formation processes is needed, which requires more numerous data on precipitation and clouds physical properties. As discussed hereafter, such requirements can be partly fulfilled by using a physically-based algorithm for the retrieval of rainfall from satellites data which offers the advantage to cover the whole Earth.

B. Problematic

Numerous instruments and methods have been developed for the measurement of precipitations. Each of them presents their own advantages and weaknesses. The simplest instrument is the well-known rain-gauge which can measure precipitation with a very high precision and accuracy. However, measurements from rain-gauge are punctual and can be spatially unrepresentative of surrounding areas. Moreover, the density of rain-gauge measurements is not satisfactory in inhabited areas, in some developing countries and, of course, over oceans. During last decades, technologies using weather radar data have been widely developed for evaluating precipitation rates. With respect to rain-gauge measurement, they show a lower accuracy but a better spatial representativeness. Main disadvantages of radar technologies are their cost and their limited observation areas (about 200 km for common C-band radar) with respect to satellites derived data. The accuracy of methods using satellites data for rainfall retrieval is lower than the one from radar-based technologies but they are also spatially representative and the areas covered are usually very wide.

Different methods have been developed to retrieve rainfall from satellites data. As it retrieves physical properties of clouds such as Cloud Optical Thickness (COT) or effective radius of cloud particles (Re), the Cloud Physical Properties (CPP) algorithm is one of the few one that is physically-based. The need for such methods is particularly justified in temperate climates where most of precipitation comes from frontal systems. Indeed, the complexity and variability of vertical profiles of frontal systems does not allow direct matching between cloud top temperatures from infrared channels and rain rates from passive microwave measurements as it is sometimes performed for convective systems over tropical regions (Todd *et al.,* 2000 ; Sorooshian *et al.,* 2002). The assessment of rain rates in frontal systems from visible and infrared satellites data requires therefore the retrieval of clouds microphysical properties such as Cloud Water Path (CWP), effective radius of droplets... However, bi-spectral methods that use visible and near-infrared data such as the CPP method cannot be used in nigh-time or in winter time over temperate areas. As a consequence, an important part of fallen precipitation cannot be measured as shown in the validation section (Figure 6). Independent radar or passive microwave/infrared method development is therefore also particularly desirable.

The CPP algorithm was first validated by Roebeling *et al.,* (2006) using ground measurements of cloud physical properties. The ability of the algorithm for the retrieval of rainfalls has been further evaluated during a 2-month comparison with weather radar from the KNMI (Koninklijk Nederlands Meteorologisch Institute) network (Roebeling & Holleman, 2009). The aim of the present study is to extend the validation over a longer climatic period (seven years) in order to assess the algorithm performances throughout yearly and daily cycle, seasonal shift of precipitation types… using data from the Belgian weather radar network from the Royal Meteorological Institute of Belgium (RMIB). Results of the present study are aimed to provide a guideline for the use of CPP data for both operational and research purposes as well as to open new perspectives of research with the creation of a seven year data set of parallax-shift corrected clouds and precipitation data.

II. METHODS

A. The CPP algorithm

Developed at the KNMI within the frame of the SAF-NWC activities, the CPP is a physically-based algorithm that uses visible and near-infrared observations from imaging radiometers. It is based on two simple physical principles. The first one assumes that reflectances in the visible channel (e.g. at 0.6 µm or 0.8 µm) do not depend on cloud particle size and are only function of Clouds Optical Thickness (COT). The second assumption is that in a near-infrared (NIR) channel, the single scattering albedo is less than 1 and depends on particle size. Reflectances measured in NIR channels (e.g. at 1.6 µm or 3.7 µm) are thus proxies for the effective radius (Re) of cloud particles. Relations between measured reflectances and COT or R_e are stored in Look-Up Tables (LUT) computed with the help of a sophisticated radiative transfer model, the DAK RTM (De Haan *et al.,* 1987; Wolters *et al.,* 2006). The DAK allows to compute corresponding reflectances at 0.6 and 1.6 µm for a large number of realistic COT or R_e values and possible geometrical configurations depending on sun and satellite positions. This model also takes into account for different optical behavior of water and ice particles. The inversion of the relationships and the interpolation in the LUT allow thus to retrieve COT and Re values from measured VIS and NIR reflectances. LUTs are built for both water and ice clouds. Clouds are considered as made of ice if the Cloud Top Temperature (CTT) is lower than 265° K and if the measured reflectances at 0.6 and 1.6 µm correspond to the simulated values for ice particles. CTT is estimated from the brightness temperature in an infrared window channel (e.g. at 10.8 µm). Once phase, optical thickness, effective radius and CTT are known, the next step consists in the computation of the Cloud Water Path (CWP, in g.m^{-2}) using

$$CWP = \frac{2}{3} \; COT.R_e.\rho_w \qquad \text{(eq. 1)}$$

Where ρ_w is the volumetric mass of liquid water. The delimitation of precipitation areas is then performed by labeling as precipitating every cloudy pixel with a CWP above a threshold value of 160 g.m^{-2}. For water clouds, an additional condition for precipitation is that the effective radius (R_e) should be larger than 15 µm.

Once the delimitation of rain areas is achieved, the next step consists in the quantitative assessment of the rain rate (R, mm.h^{-1}) as

$$R = \frac{c}{H}\left[\frac{CWP - CWP_0}{CWP_0}\right]^{\alpha} \qquad \text{(eq. 2)}$$

Where c and α are constant, CWP_0 is the threshold value for cloud water path (160 g.m^{-2}) and H, the height of the cloud column. The height of the cloud column is retrieved using the following semi-empirical relation

$$H = \left(\frac{CTT_{max} - CTT_{pix}}{6.5}\right) + dH \qquad \text{(eq. 3)}$$

Where CTT_{pix} is the cloud top temperature of the current the pixel, CTT_{max} the highest cloud top temperature in the 100x100 pixels surrounding window (which corresponds to the lowest cloud), 6.5 is the dry adiabatic lapse rate (in K/km) and *d*H is an offset value of 0.6 kilometre.

B. Satellites and Radar data

As a cloud mask is performed at first step of the CPP algorithm, data of both the visible and the infrared channels are needed for the processing. A 600 by 300 SEVIRI pixels area centered on Belgium was extracted from the RMIB archive of SEVIRI-MSG data. Due to the position of the satellite, an MSG pixel at our latitude (50° N) is about 4 x 7 kilometers. A complete data set (except for some MSG missing data) of cloud and rain properties at 15' frequency over the 2005 - 2011 period has been processed for this area using the CPP-PP algorithm.

Weather radar data archives are also stored at the RMIB. For the comparison, we used composite radar images that gather data from the RMIB weather radar in Wideumont in southern Belgium as well as data from the radar of Brussels Airport operated by Belgocontrol. From the 1st August 2008 onwards, composite images also incorporate data from a weather radar located in the Avesnois operated by MeteoFrance. Resolution

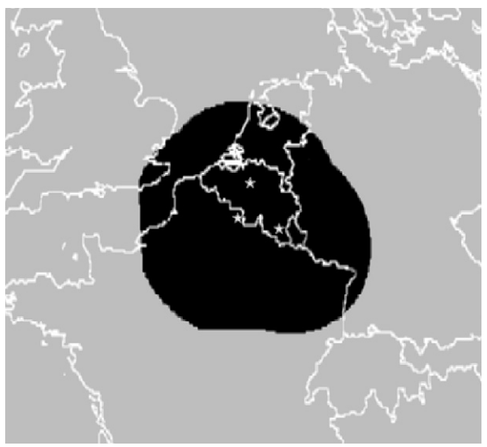

Figure 1. Location of the three radars (Zaventem, Wideumont and Avesnois) used in composite images and corresponding 240 kilometers useful radius.

of weather radar data is one kilometer and maximum reach is 240 kilometers. Location of the three radars and corresponding reach area can be seen in the first figure (Figure 1). Time mismatch has been handled by taking into account the scanning delay of the SEVIRI instrument which implies that the more suited image for the comparison with a SEVIRI slot taken at a given UTC time is the radar image taken 10 minutes later in Belgium. For validations, data of pixels located at more than 120 kilometers of any radar have not been considered due to the decreased reliability of weather radar measurements above this threshold.

C. Post-processing and parallax-shift correction

In order to be compared with SEVIRI retrieved rainfall, radar images have been converted from digital count to rain rates in $mm.h^{-1}$ and reprojected from the polar stereographic projection used for radar data to the projection used for MSG data with a consequent decrease in resolution from 1 to 5 kilometers.

For the comparison with weather radar, CPP data have been corrected from the parallax-shift effect that is a big issue for retrieved rain fall using data from geostationary satellites (Vicente *et al.,* 2002). Indeed, due to the position of the satellite, the parallax-shift towards the North can reach up to 20 kilometers at mid-latitudes for very high clouds. Therefore, real positions of clouds have been recomputed by searching the intersection between a line joining the apparent position of the cloud and the satellite with a sphere having as radius the Earth radius plus the Cloud Top Height (CTH). The CTH, in kilometers, is estimated as

$$CTH = \left(\frac{T_{surf} - CTT}{5.5} \right) \quad \text{(eq. 4)}$$

Where T_{surf} is the surface temperature (use of a monthly climatological value for Belgium), CTT is the cloud top temperature computed in the CPP algorithm and 5.5 K/km, the moist adiabatic lapse rate.

By doing such parallax-shift correction, some gaps appear. They have been filled by using information from the surroundings pixels (e.g. by taking the median value of the eight neighbouring pixels). Once these operations have been performed, a direct comparison between weather radar and CPP rain rates is possible.

III. RESULTS AND DISCUSSION

A. Delineation of precipitation areas

1. Spatial extent of precipitation

One of the simplest method to evaluate the ability of the algorithm to delineate rain areas is to compute the spatial extent of precipitation in percent, per images or over a certain period (hourly, daily, …). Results of such computation and comparison of derived statistics between spatial extent of precipitations in weather radar and CPP data sets are shown for different seasons (Table 1). In order to take into account the assumed decrease in performances of the CPP algorithm at high sun zenith angle, statistics presented in this table have been computed between 11h and 13h UTC in winter, 10h and 15h UTC in spring and 09h and 16h UTC in summer using data from the years 2009 and 2010. Overall, this comparison shows that the CPP agrees reasonably well with the radar in terms of spatial extent of precipitation. Good correlation and reasonable Root Mean Square Error (RMSE) are observed in spring and summer. Excellent statistics are found in autumn with almost perfect correlation and very low mean error. This fact should be explained by very frequent, widespread and stratiform precipitation during autumns 2009 and 2010 (mainly October and November) which can be noticed from greater mean spatial extents of precipitations and therefore, better signal to noise ratio. During these periods of recurrent of frontal precipitation in autumn, CPP algorithm has been very reliable for the assessment of precipitation areas. However, poor correlations and important errors in winter suggest an important effect of lower zenith angle in winter on CPP algorithm performances rather than the effect of the change in precipitation type.

	RADAR Mean ± STD	CPP-PP Mean ± STD	Mean Error	RMSE	Correlation
Winter (DJF)	6,47±12,23	5,64±9,74	0,84	9,03	0,69
Spring (MAM)	6,05±10,55	6,34±12,10	-0,29	6,82	0,83
Summer (JJA)	6,81±10,63	7,49±12,31	-0,68	6,06	0,87
Autumn (SON)	9,32±7,56	9,52±8,48	-0,20	1,21	0,99

Tableau 1. Mean and standard deviation of the Spatial extent of precipitation, expressed in %, of the comparison area (i.e. a 120 km radius around each radar). The results are given for the Radar and the CPP separately as well as the difference (Radar-CPP) bias, the RMS error and the correlation.

2. Contingency matrix

Another way to assess satellite-based method performances is to consider events as binary (precipitation or not) in both data set (observations and estimations) and to make the contingency matrix of the four possible events: hits (h), rain in both data sets, miss (m), rain in radar, not in CPP, false alarm (f), rain in CPP, not in radar, and correct rejections (r), no rain in both. Valuable statistics can be calculated from the frequencies of these events such as the False Alarm Ratios (FAR: f / h + f), the Probability Of Detection (POD: h / h + m) or the Critical Success Index which synthesizes information from the first two indicators and can be interpreted as the fraction of all events estimated and/or observed that were correctly diagnosed (Ebert, 2007). The CSI is computed using the following formula, (perfect score for CSI is 1):

$$CSI = \frac{h}{h + m + f} \quad \text{(eq. 5)}$$

The evolution of POD computed over a six years period (2005-2010) per month and per ranges of Sun Zenith Angles (SZA) with corresponding uncertainties is presented in the next table (Table 2). For a same SZA range, the results show few variations between each months which tends to minimize the effect of the change in precipitation types on the algorithm performances for the delimitation of precipitation areas. On the other hand, the decrease of performances SZA higher than 60° is clear for all months. Same statements can be made from the following figure, where Critical Success Index (CSI) is given as function of SZA for different spring and summer months (Figure 2). Once again, for each of these months, the decrease of CSI is significant for SZA higher than 65-70°.

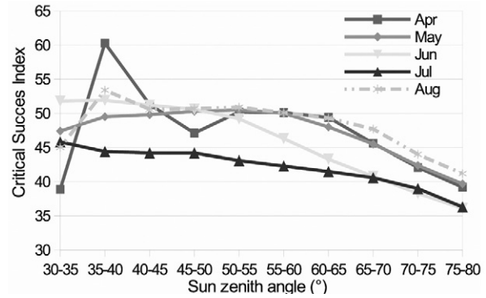

Figure 2. Critical Success Index (CSI) as a function of the sun zenith angle for different spring and summer months

B. Quantitative assessment of rain rates

1. Histogram of frequencies

Validation of the ability of the CPP algorithm to retrieve quantitative rain rate ($mm.h^{-1}$) has been first performed by verifying whether the method reproduces similar frequency distribution of such rain rates as observed in radar data or not. Next graphics show the comparison of the frequency distribution of rain rates in CPP and RADAR data from very low (0,2 - 1 $mm.h^{-1}$) to very high rain rates (20 - 50 $mm.h^{-1}$). They have been built using data from respectively winter (Figure 3) and summer (Figure 4) 2009 and 2010.

Statistics for winter months have been computed using images taken between 11h and 13h UTC and between 09h and 16h UTC for summer months. A disagreement between the CPP and the radar frequency distributions appears in winter (Figure 3) with a significant underestimation of low rain rates frequency in CPP data while high rain rates (20 - 50 $mm.h^{-1}$) are significantly over-represented with respect to radar data. These discrepancies lead to an important positive systematic bias in the CPP assessment of rain rates

POD	50-55°	55-60°	60-65°	65-70°	70-75°	75-80°
Jan				54,2 ± 0,312	45,7 ± 0,140	40,0 ± 0,222
Feb		49,0 ± 0,375	39,3 ± 0,194	48,4 ± 0,147	46,4 ± 0,174	41,9 ± 0,237
Mar	52,1 ± 0,163	56,3 ± 0,154	53,9 ± 0,181	49,9 ± 0,194	44,9 ± 0,200	41,3 ± 0,259
Apr	56,5 ± 0,227	56,2 ± 0,237	54,8 ± 0,244	50,5 ± 0,252	47,0 ± 0,253	43,7 ± 0,321
May	59,7 ± 0,187	58,6 ± 0,189	56,6 ± 0,188	54,1 ± 0,189	51,1 ± 0,188	48,8 ± 0,236
Jun	58,2 ± 0,225	55,2 ± 0,225	52,1 ± 0,225	50,0 ± 0,228	47,7 ± 0,231	45,9 ± 0,292
Jul	50,8 ± 0,195	50,1 ± 0,200	48,9 ± 0,204	47,9 ± 0,206	46,1 ± 0,208	43,6 ± 0,262
Aug	61,3 ± 0,177	59,9 ± 0,185	58,2 ± 0,188	56,2 ± 0,190	52,3 ± 0,192	49,4 ± 0,246
Sep	63,4 ± 0,264	58,2 ± 0,290	56,3 ± 0,331	49,6 ± 0,344	43,4 ± 0,356	37,2 ± 0,480
Oct	67,7 ± 0,333	58,6 ± 0,162	51,1 ± 0,113	46,3 ± 0,094	43,4 ± 0,086	40,1 ± 0,123
Nov			51,0 ± 0,499	44,3 ± 0,093	40,8 ± 0,071	38,0 ± 0,110
Dec					50,2 ± 0,125	46,8 ± 0,154
Average :	58,71 ± 0,221	55,79 ± 0,224	52,22 ± 0,237	50,13 ± 0,204	46,58 ± 0,185	43,06 ± 0,245

Tableau 2. Probability Of Detection (POD) as function of sun zenith angle computed for each calendar month over the period 2005-2010.

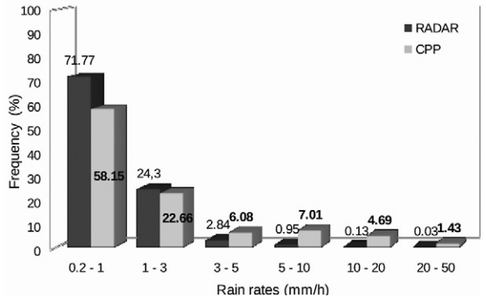

Figure 3. Histogram of frequencies of rain rates over Belgium retrieved by RADAR and CPP method for winter time (11h – 13h UTC)

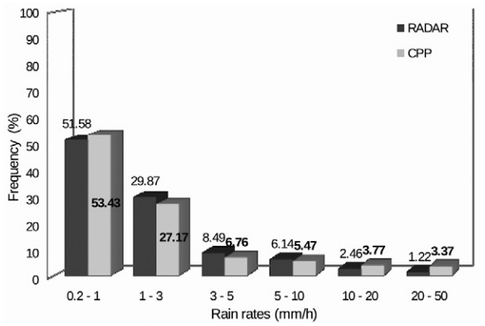

Figure 4. Histogram of frequencies of rain rates over Belgium retrieved by RADAR and CPP method for summer time (09h – 16h UTC)

in winter time. In summer time, the CPP and radar frequency distributions agree quite well (Figure 4). Only a limited overestimation remains for very high rain rates (20 - 50 mm.h^{-1}). This would suggest that the systematic overestimation of rain rates with the CPP disappear in summer time while there is still a positive bias for extremely high values.

2. Mean rain rates

Further investigations have been carried out to determine the reasons of the observed biases and errors. For the construction of the next plot (Figure 5), daily mean of rain rates per SZA ranges (therefore computed on few images) have been calculated. On this plot, the ratio of CPP/radar for median and percentile 95 of the daily mean of rain rate per SZA range have been represented. It can be seen that the ratio of the medians remains around 1.0 for most SZA excepted

	RADAR Mean ± STD	CPP-PP Mean ± STD	Mean Error
07 – 09 UTC	0,10 ± 0,28	0,21 ± 0,53	-0,105
10 – 12 UTC	0,13 ± 0,23	0,14 ± 0,27	-0,005
15 – 17 UTC	0,18 ± 0,34	0,29 ± 0,63	-0,107

Tableau 3. Mean rain rates (mm.h-1) and Mean Error (Radar - CPP) for different hours in summer time

for high values of (SZA > 65°). Above such angles, the ratio increases rapidly and becomes > 2, which suggest an important and systematic overestimation of rain rates using CPP at high SZA. Concerning the ratio of the percentiles 95, we can see that it is significantly > 1.0 for most values of SZA which suggests that the overestimation of extreme values in the CPP retrieved rainfall is present at most of sun elevation conditions. The effect of SZA values on rain rates is confirmed in next table (Table 3). In this table, we can see the good agreement between CPP and radar mean rain rates at midday in summer while there is a significant overestimation in the CPP data set with respect to radar data in early morning and late afternoon (high values of sza). For application purposes, taking into account a maximum threshold of 65° for SZA value, CPP method limitations are inspected using precipitation data for the year 2012 from Mont Rigi weather station (674 meter a.s.l) in eastern Belgium. Next plot (Figure 6) shows that on a yearly basis, only about 25% of precipitation volume falls during day-time when CPP method is suited (SZA < 65°). There are major seasonal differences with no precipitation measurement possible in winter time over temperate areas while in spring and summer, respectively 35 and 55% of the precipitation are measurable using the CPP method. For each season,

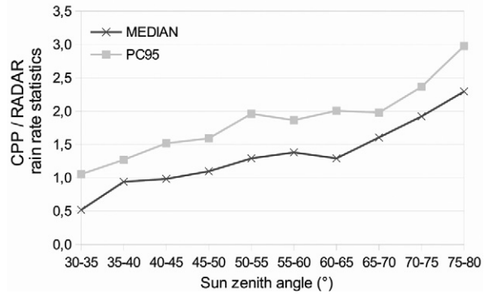

Figure 5. Ratio of CPP/RADAR of daily mean rain rate statistic as function

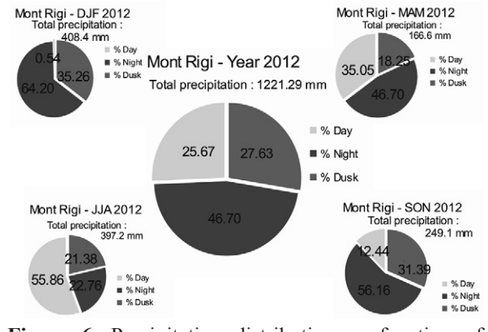

Figure 6. Precipitation distribution as function of different moment of the day for the year 2012 and for the four seasons. Day time corresponds to SZA < 65°, dusk time to 65° < SZA < 90° and night time to SZA > 90°

the amount of precipitation that falls during so-called 'dusk period' (65° < SZA < 90°) is non negligible.

Our results are consistent with the fact that the quality of satellite retrievals decreases in general at high SZA values. For the measurement of cloud physical properties and, as consequence in this case, rainfalls, this fact can be explained by reduced incoming solar radiations, more important shadow effects from cloud tops and increased horizontal transfer of photons between neighboring pixels for low sun elevation conditions. The overestimation of extreme values of precipitation using the CPP algorithm has also been observed and could be explained by the higher sensitivity to radiometric errors of the instrument in the visible channel (0.6 µm) which affects the retrieval of cloud optical thickness and thus of CWP. Roebeling *et al.* (2006) have concluded that the SEVIRI instrument saturates for clouds with a CWP > 700 g.m^{-2}. This increased sensitivity to radiometric errors for very thick clouds has been highlighted by the study of Cattani *et al.,* (2007) where major uncertainties for water clouds with a COT > 100 have been found for a typical instrument error on visible reflectance of 5 %. To deal with this, Roebeling & Holleman (2009) have proposed a fixed maximum value of 40 mm.h^{-1} when using CPP algorithm with SEVIRI data in order to dismiss excessive and unrealistic high values of rain rates.

IV. APPLICATION: DATA ON CLOUDS MICROPHYSICS

A. Effective radius and optical thickness of maritime and continental clouds

Thanks to the computation of clouds properties as steps for the assessment of rain rates, interesting plots and graphics can be made in order to study clouds processes as well as their temporal and spatial variations. A first example is given where one can see the mean effective radius, Re, of water clouds for the month of August 2008 (Figure 7). Significant differences can be seen between near-coast inland areas (Western France and Belgium, the British Isles, West coasts of Scandinavia…) where Re of water clouds is greater (between 12 and 15 µm) than for maritime as well as more continental areas (9 - 11 µm). This difference might be explained by the aerosol load that clouds experience during their travel over lands. Therefore, over continental areas, condensate water is distributed over a greater number of clouds condensation nuclei which express their lower mean radius. On the other hand, over coastal areas, the reduced numbers of aerosols permit more frequently the growth of water particles under the freezing level thanks to warm rain processes (coalescence). However, aside from this climatic effect, cares are to be taken. Indeed, some land features (islands, estuaries...) are too sharp to be explained by differences in cloud properties over land and maritime surfaces. This fact should actually be the consequence of a poor treatment of the surface-reflected shortwave radiation. A better representation of the land and ocean albedo should therefore be introduced to reduce this ocean-land jump.

Concerning optical thickness, we can observe similar spatial patterns as for effective radius (Figure 8). Coastal land areas of Northwestern Europe, Southern Scandinavia and the British Isles experience optically thicker clouds as far as water clouds are considered. This can be partly explained by the triggering of convection in maritime air masses when arriving over land areas (August 2008 has been dominated by moist westerly flows over Northern Europe). More southern or more continental areas have lower COT values for water clouds thanks to more favorable weather and more frequent ice clouds when convection occurs. The effect of updrafts generated by mountains and high grounds is also obvious with increased optical thickness of water clouds over the Massif Central and some parts of the Alps. The effect of topography is even sharper over the British Isles with optical thickness peaking at the very location of topography summits. There gain, too obvious contrast over some land features witness an "albedo artifact" as reflection from underlying surfaces is not properly treated.

B. Non-precipitating clouds

Another example of research that can be carried out with cloud microphysics data is presented (Figure 6). This figure shows the relative frequency over Western and Central Europe of non precipitating water clouds in winter (top) and summer 2008 (bottom). According to Roebeling & Holleman (2009), non precipitating clouds are defined as clouds with an unusually small effective radius (Re < 15 µm) with respect to their high Cloud Water Path (CWP > 160 g.m^{-2}). These clouds can either be the result of strong updrafts or strong natural or anthropic aerosol loads possibly due to anthropic pollution. Indeed, as we have seen, aerosol loads distribute condensed water over a greater number of particles which reduces the size of particles (Bréon *et al.,* 2002), delays the onset of precipitations and therefore cloud clearance which is known as the indirect aerosol effect (Rosenfeld *et al.,* 2008). Strong updrafts, usually produced by the combination of instability and orographic ascendance, can rapidly bring particles to upper parts of the atmosphere without allowing time for warm rain processes to take place. On the summer plot, we can see that non-precipitating clouds occur mainly over the Alps and the high grounds of the British Isles and Ireland suggesting an effect of strong updrafts. An increased frequency of non-precipitating clouds is also observed over Northwestern France, Belgium and the Netherlands. While this observation might be the results of aerosols load, possibly anthropic pollutions,

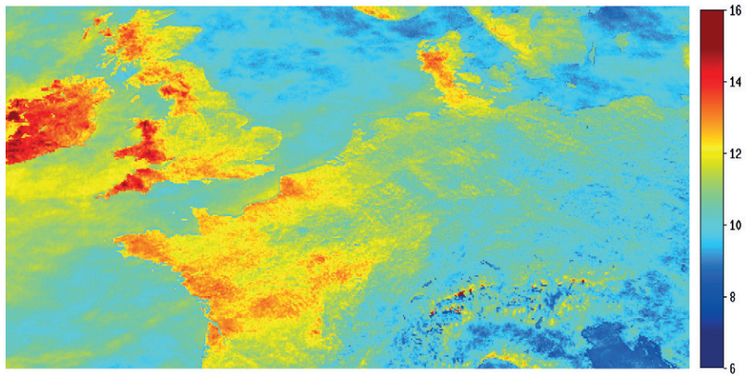

Figure 7. Mean effective radius (in µm) of water clouds for August 2008

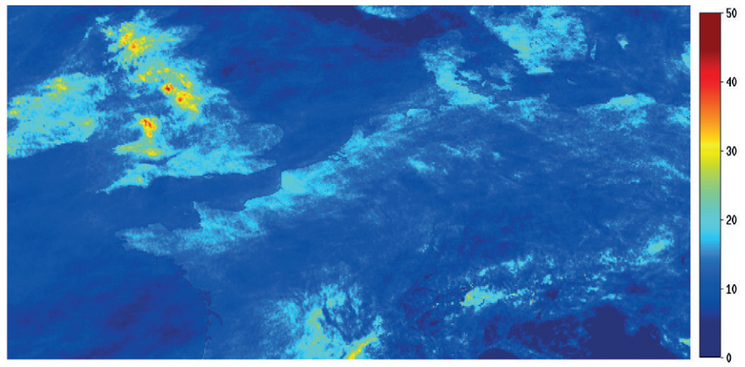

Figure 8. Mean optical thickness of water clouds for August 2008

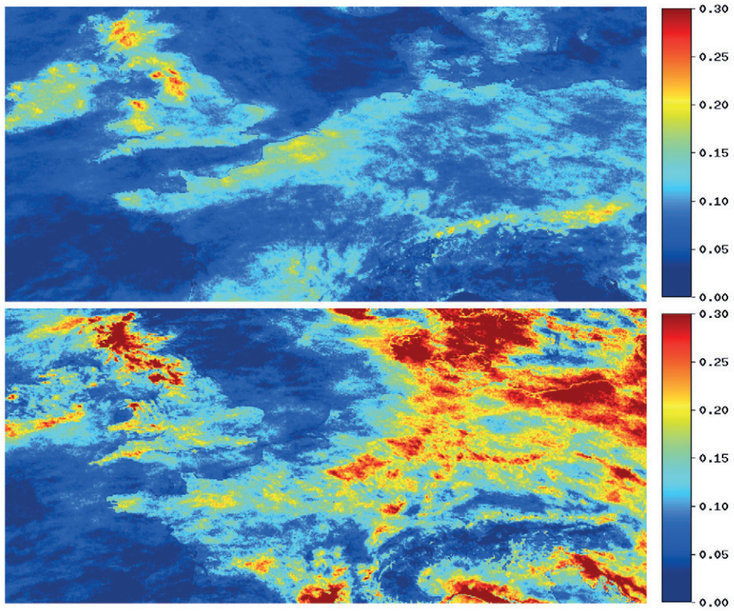

Figure 9. Frequency of non-precipitating clouds (Re < 14µm & CWP > 160 g.m-2) for summer months (top) and winter months (bottom)

this hypothesis does not explain why no increased frequency of non precipitating clouds is observed in summer over other industrial areas like Germany or Poland. Moreover, due to frequent thermal updrafts over continental areas in summer, and more frequent occurrence of ice processes in aerosol loaded cloud masses, a study of ice clouds should be more interesting for the tracking of aerosol loads effects in summer.

In the winter plot (Figure 9), major differences are noticeable with a strong occurrence of non-precipitating clouds in Eastern Belgium, Germany, Poland and Scandinavia. These non-precipitating clouds might be the result of frequent low cloudiness in winter time in combination with important aerosols emissions trapped under subsidence inversions. However, not much confidence should be accorded to this winter plot given the limited performances of the CPP retrievals at high SZA conditions. The interest of studying water clouds in winter might also be questioned as their representativeness is reduced in some areas like over the Alps where a frequency of non-precipitating water clouds close to zero can be observed on the plot as most clouds over this area in winter should be made of ice.

V. CONCLUSIONS AND PERSPECTIVES

The study has shown the ability of the CPP algorithm to capture precipitation areas. Thanks to weak sensitivity of the threshold values to instrument calibration and noise, the delimitation of precipitation areas remains reliable until SZA up to 65°. Nevertheless, the quantitative assessment of rain rates is more sensitive to SZA. Indeed, an important overestimation using CPP output from SEVIRI data appears at SZA higher than 60° and increases rapidly towards high values of SZA. Therefore the use of this method is seriously compromised for the winter half of the year at mid-latitudes as well as in early morning and late afternoon during summer. Besides, due to greater sensitivity to instrument errors for the retrieval of high value of cloud optical thickness and Cloud Water Path (CWP > 700 $g.m^{-2}$), there is a systematic overestimation of extreme precipitation events.

The study highlights that some improvements are still needed in the algorithm. In particular, a better treatment of land and oceanic surfaces albedo is desirable in order to reduce the effect of surface reflection which seems to contaminate the retrieval of clouds physical properties. Results are however very encouraging and it is important to point out that most of the observed limitations come from instrument radiometric errors, particularly when using instrument on-board geostationary satellites such as SEVIRI. Therefore, it is clearly worth to continue the development of such algorithm as reduced instrument errors, increased spatial resolution and increased number of spectral channels are expected with the next generations of geostationary satellites radiometers (e.g. Flexible Combined Imager on board Meteosat Third Generation).

Current performances of CPP algorithm are however found to be sufficient to allow atmospheric researches, as well as validation or even data assimilation purposes with numerical models, provided the limitations for the application of the algorithm are properly taken into account. Indeed, despite reduced accuracy with respect to other methods, the covered areas, the resolution (3 to 5 kilometers) and the time sampling (every 15 minutes) are undeniable advantages for the acquisition of precipitation data over areas poorly covered by other methods of precipitation measurements. The computation of reliable data on cloud physical properties is also extremely interesting for research purposes given the usual low availability of such data.

ACKNOWLEDGMENTS

The authors want to express their gratitude to Jan Fokke Meirink from KNMI for providing the CPP code, his help and advices. Advices from Rob Roebeling from EUMETSAT have also been very valuables. Sincere acknowledgments are also due to Laurent Delobbe and Christophe Ferauge for providing access to the weather radar data of the RMIB and attached recommendations.

BIBLIOGRAPHY

Alexander L. V., Zhang X., Peterson T.C., Caeser J., Gleason B., Klein Tank A.M.G., Haylock M., Collins D., Trewin B., Rahimzadeh F., Tagipour A., Rupa Kuma K., Revadekar J., Griffiths G., Vincent L., Stephenson D.B., Burn, J., Aguilar E., Brunet M., Taylor M., New M., Zhai P., Rusticucci M., Vazquez-Aguirre J.L. (2006). Global observed changes in daily climate extremes of temperature and precipitation. *J. of Geophys. Res*., 111, D05109.

Breon F., Tanre D. & Generoso S. (2002). Aerosol Effects on Cloud Droplet. *Science*, 295, 834-838.

Cattani E., Melani S., Levizzani V. & Costa J.M. (2007). The retrieval of cloud top properties using VIS IR channels. In *Measuring precipitation from space*, *EURAINSAT and the future*, Advances in Global Change Research, 28, Springer, Dordrecht, pp. 79-96.

De Haan J.F., Bosma P.B. & Hovenier J.W. (1987). The adding method for multiple scattering calculations of polarized light. *Astron. Astrophys*., 183, 371-391.

Ebert E.E. (2007). Methods for verifying satellite precipitation estimates. In *Measuring precipitation from space, EURAINSAT and the future*, Advances in Global Change Research, 28, Springer, Dordrecht,

pp. 345-356.
Lehner B., Doell P., Alcamo J., Henrichs T. & Kaspar F. (2006). Estimating the impact of global change on flood and drought risks in Europe : A continental, integrated Analysis. *Climatic Change*, 75.3, 273-299.
Roebeling R. & Holleman I. (2009). SEVIRI rainfall retrieval and validation using weather radar observations. *Journal of Geophysical Researches*, 114, D21202, doi:10.1029/2009JD012102.
Roebeling R., Feijt A.J. & Stammes P. (2006). Cloud property retrieval for climate monitoring : Implications of differences between Spinning Enhanced Visible and Infrared Imager on METEOSAT-8 and Advanced Very High Resolution Radiometer (AVHRR) on NOAA-17. *Journal of Geophysical Researches*, 111, D20210, doi:10.1029/2005JD006990.
Roebeling R., Deneke H.M. & Feijt A.J. (2008). Validation of Cloud Liquid Water Path Retrievals from SEVIRI using one year of CloudNet Observations. *Journal of applied Meteorology and Climatology*, 47, 206-222.
Rosenfeld D., Lohmann U., Raga G.B., O'Dowd C.D., Kulmala M., Fuzzi S., Reissell A., Anderae M.O. (2008). Flood or Drought: How do aerosols affect precipitation? *Science*, 321, 1309-1313.
Sooroshian S., Gao X., Hsu K., Maddox R.A., Hong Y., Gupta H.V. & Imam B. (2002). Diurnal Variability of Tropical Rainfall Retrieved from combined GOES and TRMM Satellite Information. *Journal of Climate*, 15, 983-1001.
Todd T.C., Kidd C., Kniveton D. & Bellerbry T.J. (2001). A Combined Satellite Infrared and Passive Microwave Technique for Estimation of Small-Scale Rainfall. *Journal of atmospheric and oceanic technology*, 18, 742-755.
Trenberth K.E., Jones P.D., Ambenje P., Bojariu R., Easterling D., Klein Tank A., Parker D., Rahimzadeh F., Renwick J.A., Rusticucci M., So-den B. & Zhai P. (2007). Observations: Surface and Atmospheric Climate Change. In S. Solomon., D. Qin, M. Manning, Z. Chen, M. Marquis, K.B. Averyt, M. Tignor and H.L. Miller (eds.), *Climate Change 2007: The Physical Science Basis. Contribution of Working Group I to the Fourth Assessment Report of the Intergovernmental Panel on Climate Change*. (chap. 3, 235-336). Cambridge, Cambridge University Press.
Twomey, S. (1991). Aerosols, clouds and radiation. Atmospheric Environment. Part A. *General Topics*, 25, 2435-2442
Vicente G.A., Davenport J.C. & Scofield R.A (2002). The role of orographic and parallax corrections on real time high resolution satellite rainfall rate distribution. *Int. J. Remote Sensing*, 23, 221-230.
Wolters E.L.A., Roebeling R.A. & Stammes P. (2006). *Cloud reflectance calculations using DAK : study on required integration points*. Technical report, TR 292. De Bilt, KNMI.

Coordonnées des auteurs :

Julien BEAUMET, Xavier FETTWEIS
& Michel ERPICUM
Université de Liège,
Unité de Topoclimatologie et Climatologie,
Sart-Tilman, Bât.20,B-4000 Liège
julien.beaumet@ulg.ac.be, Xavier.Fettweis@ulg.ac.be, michel.erpicum@ulg.ac.be

Nicolas CLERBAUX
Royal Meteorological Institute of Belgium,
Section Remote Sensing from Space,
Avenue Circulaire 3, B-1180 Bruxelles
Nicolas.Clerbaux@oma.be

BSGLg, 61, 2013, 15-36

FLUX DES SEDIMENTS EN SUSPENSION DANS LES RIVIERES DU BASSIN DE LA MEUSE : PROPOSITION D'UNE TYPOLOGIE REGIONALE BASEE SUR LA DENUDATION SPECIFIQUE DES BASSINS VERSANTS

Jean VAN CAMPENHOUT, Anne-Cécile DENIS, Eric HALLOT, Geoffrey HOUBRECHTS, Yannick LEVECQ, Alexandre PEETERS & François PETIT

Résumé
L'érosion des sols peut être appréhendée à l'échelle du bassin versant en quantifiant le transport sédimentaire en suspension à son exutoire. Environ 2.000 mesures de concentration des matières en suspension ont permis d'estimer le transport sédimentaire annuel au niveau de 80 stations situées en région wallonne, à l'exutoire de bassins versants d'une superficie de 16 à 2.900 km². Des différenciations régionales ont pu être mises en évidence en fonction du substrat et de l'occupation du sol des bassins versants. À l'échelle régionale, le taux de dénudation annuel moyen atteint 20 t.km-2.an-1 en Lorraine, 34 t.km-2.an-1 en Ardenne et 69 t.km-2.an-1 dans l'Entre-Vesdre-et-Meuse. La granulométrie des particules transportées et la proportion de matière organique complètent l'analyse et montrent également une différenciation selon les régions agro-géographiques. Des données issues d'autres travaux académiques ou administratifs ont été intégrées à la base de données afin de définir les meilleurs sites de mesure en continu de la concentration des matières en suspension en Wallonie.

Mots-clés
concentration des sédiments en suspension, érosion des sols, analyse granulométrique, matière organique, dénudation spécifique, bassin de la Meuse, Ardenne

Abstract
Soil erosion may be apprehended at the watershed scale by quantifying the transport of suspended sediment at its outlet. Approximately 2000 measurements of suspended sediment concentration were used to estimate the annual sediment discharge at 80 stations located in the Walloon region (Belgium), at the outlet of watershed from 16 to 2900 km². Some regional differences have been highlighted depending on the substrate and the land use in the watershed. At the region scale, the mean annual sediment yield reaches 20 t.km-2.yr-1 in Lorraine, 34 t.km-2.yr-1 in Ardenne and 69 t.km-2.yr-1in Entre-Vesdre-et-Meuse. The size of suspended particles and the proportion of organic matter also show differences between each agro-geographical area. Data from other academic or administrative works were incorporated into the database to identify the best sites for continuous measuring of the suspended load concentration in Wallonia.

Keywords
suspended load concentration, soil erosion, particle size analysis, organic matter, specific denudation, Meuse basin, Ardennes

I. INTRODUCTION

Les rivières apparaissent comme un intégrateur de la dénudation de leur bassin hydrographique. Lorsqu'elle est réduite à une surface (la taille du bassin versant), on parle alors de dénudation spécifique et s'exprime en t.km-2.an-1 ou encore en mm/millénaire (ou par an). La dénudation est estimée par la mesure du flux exporté qui se fait selon trois modes de transport : en solution, en suspension et transport de la charge de fond, qui se fait elle-même par progression du matériau par roulage et/ou saltation sur le fond du lit (Tricart, 1961).

L'importance relative de ces trois modes de transport est tout d'abord fonction du système morpho-climatique (c'est-à-dire de l'ensemble des processus qui permettent la production de sédiments et leur arrivée jusqu'aux rivières). La nature et la quantité de sédiments évacués dépend aussi de l'affectation du sol (protection plus ou moins efficace du sol par la végétation), de la lithologie et des caractéristiques géomorphologiques des bassins versants (pente, incision dans des surfaces d'érosion, contact avec les versants, …).

De façon générale, la charge de fond, malgré le rôle considérable qu'elle joue dans les problèmes de profil d'équilibre et de stabilité des lits, n'entre que pour une part négligeable dans le flux sédimentaire, excepté dans des conditions particulières, en fonction notamment de la disponibilité des matériaux et de la proximité